Journal of Advanced Ceramics
2020, **9**(4): 454–461
https://doi.org/10.1007/s40145-020-0388-3
ISSN 2226-4108
CN 10-1154/TQ

Research Article

Preparation and heat insulating capacity of $Sm_2Zr_2O_7$–SiC composites based on photon thermal transport

Zhuang MA[a,b], Qi ZHANG[a,b], Ling LIU[a,b,*], Yanbo LIU[a,b]

[a]*School of Materials Science and Engineering, Beijing Institute of Technology, Beijing 100081, China*
[b]*Beijing Institute of Technology Chongqing Innovation Center, Chongqing 401120, China*

Received: December 31, 2019; Revised: May 20, 2020; Accepted: May 20, 2020

Abstract: A series of $Sm_2Zr_2O_7$–SiC composites doped with different volume fraction and particle size of SiC were prepared by hot pressing at 1300 ℃. The phase of the composites prepared is P-$Sm_2Zr_2O_7$ and C-SiC, and no other diffraction peaks exist, which indicates that $Sm_2Zr_2O_7$ has great chemical compatibility with SiC. The thermal conductivity and phonon thermal conductivity of the $Sm_2Zr_2O_7$–SiC composites are measured by the laser pulse method. The photon thermal conductivity of the composites is obtained by subtracting the phonon thermal conductivity from the total thermal conductivity. The results show that the photon thermal conductivity of $Sm_2Zr_2O_7$–SiC composites is lower than that of pure $Sm_2Zr_2O_7$. The photon thermal conductivity of $Sm_2Zr_2O_7$–SiC composites decreases first and then increases with the increase of SiC particle size. $Sm_2Zr_2O_7$–(5 vol%, 10 μm)SiC composite has the lowest photon thermal conductivity.

Keywords: rare-earth zirconates; thermal conductivity; photon thermal transport

1 Introduction

Thermal barrier coatings (TBCs) are widely used to protect the hot-section components of gas turbines from hot gases [1]. With the development of aero-engine to high thrust weight ratio and high inlet temperature, the requirements for thermal insulation performance of TBCs will also be improved. In TBCs, heat is conducted by lattice vibration (phonons) or radiation (photons). TBCs with low phonon thermal conductivity are widely studied. The thermal conductivity of the high-entropy ceramics thermal barrier coatings can be 1.0 W/(m·K) due to strong phonon scattering [2]. The photon thermal conductivity component can become a significant portion of the overall thermal conductivity at elevated temperatures. However, there are relatively few reports on the photon thermal conductivity [3]. As a result, with the gas temperature increasing, it is very important for ensuring the heat insulation capacity of TBCs under high temperatures. However, most ceramic materials are semi-transparent to infrared radiation under high temperature, and thus thermal conductivity will recover rapidly. Rare-earth zirconates, such as $Sm_2Zr_2O_7$, whose thermal conductivity is lower than that of traditional yttria partially stabilized zirconia (YSZ), have the potential to be a novel candidate material for TBCs [4,5]. It was reported that the thermal conductivity of rare-earth zirconates recovered above 800 ℃ because of infrared radiation, and their thermal insulation performance decreased by about 10% than that at low temperatures [6].

* Corresponding author.
E-mail: richard@bit.edu.cn

To improve the heat insulation of rare-earth zirconates, an effort must be undertaken to increase the photon scattering occurred in the materials, which results in the photon thermal conductivity reducing. However, the method for phonon scattering (such as increasing crystal defects) is useless to reduce the photon thermal conductivity. The difference of refractive index between different materials is the main factor to increase the photon scattering and reduce the photon thermal conductivity. Besides, according to the research by Klemens and Gell [7], when the size of the defect (or the second phase) is greater than or equal to the photon wavelength, a substantial transition of the photon thermal conduction in the thermal conductivity can be made. However, no related experimental literature were reported. We have found that SiC material has good high-temperature chemical stability, and its refractive index (about 2.67) is different from the refractive index of $Sm_2Zr_2O_7$ ceramics (about 2.1), so a series of composites with different volume fraction and different particle size of SiC were prepared. In this study, the thermal conductivity of the $Sm_2Zr_2O_7$–SiC composites was investigated and compared with that of pure $Sm_2Zr_2O_7$ ceramic.

2 Experimental

2. 1 Preparation of $Sm_2Zr_2O_7$–SiC composites

The main raw materials were SiC (⩾ 99.9%, Beijing Zhongjin Research New Material Technology Co., Ltd., China), Sm_2O_3 (⩾ 99.9%, Huizhou Ruier Chemicals Technology Limited Company of Guangdong, China) and $ZrOCl_2 \cdot 8H_2O$ (⩾ 99.5%, Fanmeiya Materials Limited Company of Jiangxi, China). $Sm_2Zr_2O_7$ powders were synthesized by a chemical co-precipitation method as shown in Ref. [8]. The appropriate amount of $Sm_2Zr_2O_7$ and SiC was prepared by mechanical ball milling for 6 h. $Sm_2Zr_2O_7$–SiC composites were prepared by hot pressing at 1300 ℃ for 1 h at a heating rate of 10 ℃/min and a pressure of 200 MPa. In order to prevent the oxidation of SiC powders, the sintering process was carried out in an argon atmosphere.

2. 2 Analysis and characterization

The phase compositions of $Sm_2Zr_2O_7$–SiC composites were determined by X-ray diffraction (XRD, RIGAKU D/Max-rB, Rigaku International Corp., Japan) with the scan rate of 4 (°)/min. The microstructure of the sintered composites was examined using scanning electron microscope (SEM, Philips S-4800, Hitachi Ltd., Yoshida-Cho, Totsuka-Ku, Yokohama, Japan). The compositions of the bulks were analyzed by an energy spectrum analyzer (EDS, X-Max, Oxford Instruments plc, UK).

Since the photon thermal conductivity of ceramics cannot be measured directly, according to the heat transfer theory of ceramic material, the photon thermal conductivity of crystalline materials (k_r) can be expressed by Eq. (1):

$$k_r = k - k_p \quad (1)$$

where k and k_p represent the total thermal conductivity and phonon thermal conductivity of the material, respectively. The total thermal conductivity of the ceramics can be acquired by Eq. (2).

$$k = C_p \lambda \rho \quad (2)$$

$$C_p = A + B \times 10^{-3} T + C \times 10^5 T^{-2} + D \times 10^{-6} T^2 + E \times 10^8 T^{-3} \quad (3)$$

where the thermal diffusivity (λ) is measured by the laser pulse method (model: FLASHLINE 5000) from 25 to 1400 ℃. The specific heat (C_p) is calculated using Eq. (3) [9–11], and the parameters are obtained from Ref. [11] and shown in Table 1, where *A*, *B*, *C*, *D*, and *E* are empirical constants. The density (ρ) is measured according to the Archimedes principle. *T* is the temperature.

The phonon thermal conductivity is the same as the total thermal conductivity test. It is necessary to add a thin platinum absorbing layer between the sample surface and the graphite layer to prevent laser beam penetration into the interior of the sample and to ensure an effective and uniform absorption of the laser pulse as shown in Ref. [12]. Moreover, a platinum layer has a relatively low emissivity which reduces the amount of heat radiation emitted into the sample. The Pt layer was prepared according to the method described in Ref. [13]. Thus, most photons are blocked by the platinum absorbing layer. The phonon thermal conductivity of composites is acquired. The test schematic is shown in

Table 1 Parameters for the specific heat calculation

Parameter	*A*	*B*	*C*	*D*	*E*
$Sm_2Zr_2O_7$	267.776	34.309	–46.024	0	0
SiC	50.794	1.925	–49.204	0	8.201

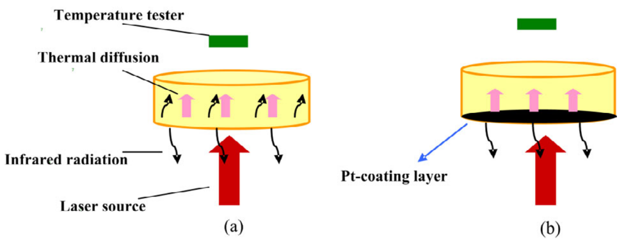

Fig. 1 Illustration of laser pulse sample test (a) without Pt-coating layer and (b) with Pt-coating layer.

Fig. 1 Finally, the photon thermal conductivity of $Sm_2Zr_2O_7$ and $Sm_2Zr_2O_7$–SiC composites can be acquired by Eq. (2).

3 Results and discussion

Figure 2 shows the XRD patterns of $Sm_2Zr_2O_7$–SiC composites with different volume and different particle size of SiC. It can be seen that the diffraction peaks of the pyrochlore structure are in good agreement with the standard peaks. Meanwhile, obvious SiC phase is observed in the spectrum, and no other phase exists. It is shown that the second phase SiC does not react with the $Sm_2Zr_2O_7$ matrix, which indicates that $Sm_2Zr_2O_7$ and SiC show good phase stability under the sintering process.

Figure 3 shows the microstructure of $Sm_2Zr_2O_7$–(10 vol%)SiC composites with SiC particle sizes of 2, 10, and 15 μm, respectively. It can be seen that SiC particles show uniform distribution in the matrix and no other grain appears. The relative densities of a series of $Sm_2Zr_2O_7$–SiC composites measured by the Archimedes principle are all above 97%. The results of element distribution in Fig. 4 show that there is no element diffusion phenomenon, and thus there is no reaction between SiC and $Sm_2Zr_2O_7$ matrix, which is consistent with the results of the XRD phase analysis.

Tables 2 and 3 show the total thermal diffusivity and phonon thermal diffusivity of $Sm_2Zr_2O_7$ and $Sm_2Zr_2O_7$–SiC composites. All data were averaged over three measurements. Table 4 shows the densities of the samples. The specific heat calculated by Eq. (3) is shown in Fig. 5. The total thermal conductivity and photon thermal conductivity were calculated according to Eqs. (1) and (2), which are shown in Tables 5 and 6. It can be seen that $Sm_2Zr_2O_7$–(5 vol%, 10 μm)SiC composite has the lowest photon thermal conductivity, compared with the single-phase $Sm_2Zr_2O_7$ at each temperature. Figure 6 shows the photon thermal

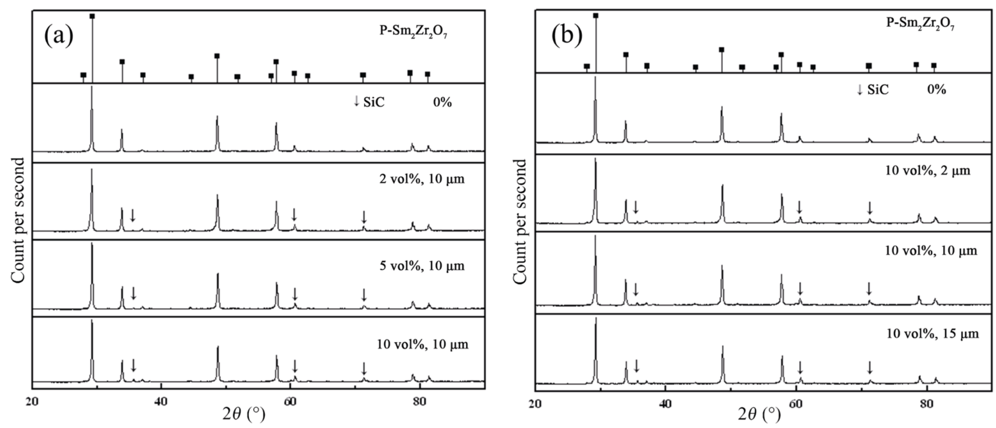

Fig. 2 XRD patterns of $Sm_2Zr_2O_7$–SiC composites: (a) SiC particle size is 10 μm with different volume and (b) SiC content is 10 vol% with different particle size.

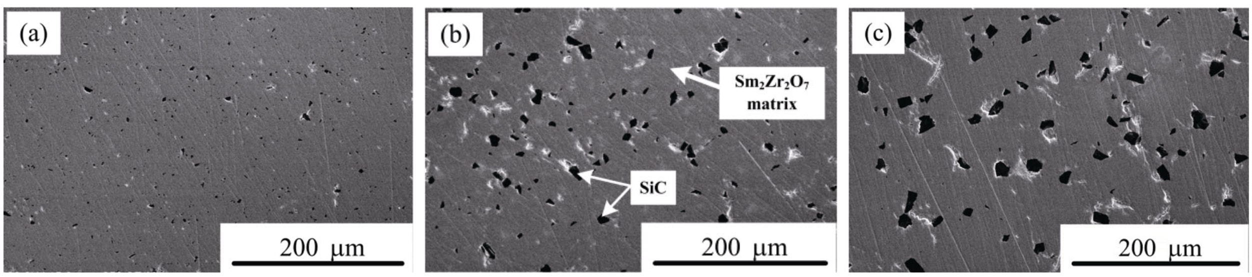

Fig. 3 Microstructures of $Sm_2Zr_2O_7$–SiC composites doping with different particle size of SiC: (a) 2 μm, (b) 10 μm, and (c) 15 μm.

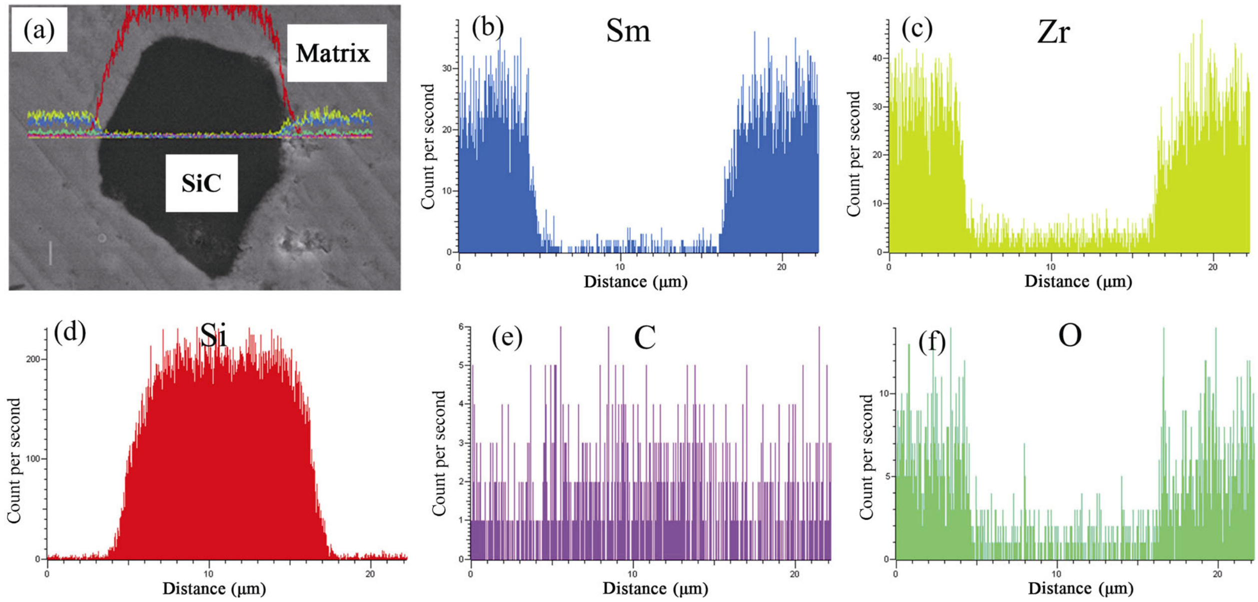

Fig. 4 Line scanning EDS analysis at the interface between SiC and $Sm_2Zr_2O_7$: (a) SEM image, (b) Sm, (c) Zr, (d) Si, (e) C, and (f) O.

Table 2 Total thermal diffusivity of $Sm_2Zr_2O_7$ and $Sm_2Zr_2O_7$–SiC composites

Sample	600 ℃	800 ℃	1000 ℃	1200 ℃
$Sm_2Zr_2O_7$	0.560	0.556	0.551	0.532
$Sm_2Zr_2O_7$–(2 vol%, 2 μm)SiC	0.485	0.484	0.497	0.512
$Sm_2Zr_2O_7$–(2 vol%, 10 μm)SiC	0.494	0.473	0.471	0.469
$Sm_2Zr_2O_7$–(2 vol%, 15 μm)SiC	0.530	0.576	0.661	0.789
$Sm_2Zr_2O_7$–(5 vol%, 2 μm)SiC	0.461	0.457	0.458	0.456
$Sm_2Zr_2O_7$–(5 vol%, 10 μm)SiC	0.460	0.464	0.459	0.466
$Sm_2Zr_2O_7$–(5 vol%, 15 μm)SiC	0.515	0.491	0.480	0.470
$Sm_2Zr_2O_7$–(10 vol%, 2 μm)SiC	0.456	0.462	0.456	0.470
$Sm_2Zr_2O_7$–(10 vol%, 10 μm)SiC	0.564	0.534	0.516	0.504
$Sm_2Zr_2O_7$–(10 vol%, 15 μm)SiC	0.575	0.574	0.586	0.605

Table 3 Phonon thermal diffusivity of $Sm_2Zr_2O_7$ and $Sm_2Zr_2O_7$–SiC composites

Sample	600 ℃	800 ℃	1000 ℃	1200 ℃
$Sm_2Zr_2O_7$	0.543	0.538	0.530	0.528
$Sm_2Zr_2O_7$–(2 vol%, 2 μm)SiC	0.433	0.405	0.383	0.378
$Sm_2Zr_2O_7$–(2 vol%, 10 μm)SiC	0.496	0.480	0.448	0.422
$Sm_2Zr_2O_7$–(2 vol%, 15 μm)SiC	0.454	0.439	0.406	0.394
$Sm_2Zr_2O_7$–(5 vol%, 2 μm)SiC	0.520	0.490	0.463	0.449
$Sm_2Zr_2O_7$–(5 vol%, 10 μm)SiC	0.469	0.440	0.417	0.404
$Sm_2Zr_2O_7$–(5 vol%, 15 μm)SiC	0.473	0.446	0.424	0.412
$Sm_2Zr_2O_7$–(10 vol%, 2 μm)SiC	0.472	0.446	0.422	0.408
$Sm_2Zr_2O_7$–(10 vol%, 10 μm)SiC	0.543	0.510	0.483	0.467
$Sm_2Zr_2O_7$–(10 vol%, 15 μm)SiC	0.518	0.487	0.458	0.440

Table 4 Density of $Sm_2Zr_2O_7$ and $Sm_2Zr_2O_7$–SiC composites

Sample	Measured density (g/cm^3)	Theoretical density (g/cm^3)
$Sm_2Zr_2O_7$	6.4649	6.6580
$Sm_2Zr_2O_7$–(2 vol%, 2 μm)SiC	6.4902	6.5892
$Sm_2Zr_2O_7$–(2 vol%, 10 μm)SiC	6.4798	6.5892
$Sm_2Zr_2O_7$–(2 vol%, 15 μm)SiC	6.4336	6.5892
$Sm_2Zr_2O_7$–(5 vol%, 2 μm)SiC	6.3538	6.4861
$Sm_2Zr_2O_7$–(5 vol%, 10 μm)SiC	6.4125	6.4861
$Sm_2Zr_2O_7$–(5 vol%, 15 μm)SiC	6.3147	6.4861
$Sm_2Zr_2O_7$–(10 vol%, 2 μm)SiC	6.1584	6.3142
$Sm_2Zr_2O_7$–(10 vol%, 10 μm)SiC	6.1442	6.3142
$Sm_2Zr_2O_7$–(10 vol%, 15 μm)SiC	6.1842	6.3142

Table 5 Total thermal conductivity of $Sm_2Zr_2O_7$ and $Sm_2Zr_2O_7$–SiC composites (W/(m·K))

Sample	600 ℃	800 ℃	1000 ℃	1200 ℃
$Sm_2Zr_2O_7$	1.8312	1.8949	1.9331	1.9576
$Sm_2Zr_2O_7$–(2 vol%, 2 μm)SiC	1.5832	1.5734	1.656	1.6662
$Sm_2Zr_2O_7$–(2 vol%, 10 μm)SiC	1.5641	1.6168	1.703	1.7812
$Sm_2Zr_2O_7$–(2 vol%, 15 μm)SiC	1.6655	1.7081	1.7412	1.7701
$Sm_2Zr_2O_7$–(5 vol%, 2 μm)SiC	1.4915	1.5269	1.5843	1.5984
$Sm_2Zr_2O_7$–(5 vol%, 10 μm)SiC	1.5064	1.574	1.6159	1.668
$Sm_2Zr_2O_7$–(5 vol%, 15 μm)SiC	1.591	1.6058	1.6254	1.6327
$Sm_2Zr_2O_7$–(10 vol%, 2 μm)SiC	1.5008	1.562	1.6269	1.644
$Sm_2Zr_2O_7$–(10 vol%, 10 μm)SiC	1.7985	1.8109	1.8532	1.8603
$Sm_2Zr_2O_7$–(10 vol%, 15 μm)SiC	1.8041	1.8211	1.8995	1.9022

Table 6 Photon thermal conductivity of $Sm_2Zr_2O_7$ and $Sm_2Zr_2O_7$–SiC composites (W/(m·K))

Sample	600 ℃	800 ℃	1000 ℃	1200 ℃
$Sm_2Zr_2O_7$	0.0461	0.1626	0.2361	0.2863
$Sm_2Zr_2O_7$–(2 vol%, 2 μm)SiC	0.0556	0.1603	0.2214	0.2742
$Sm_2Zr_2O_7$–(2 vol%, 10 μm)SiC	0.0285	0.0771	0.1371	0.1658
$Sm_2Zr_2O_7$–(2 vol%, 15 μm)SiC	0.0727	0.1048	0.1532	0.2212
$Sm_2Zr_2O_7$–(5 vol%, 2 μm)SiC	0.0906	0.1721	0.2606	0.2999
$Sm_2Zr_2O_7$–(5 vol%, 10 μm)SiC	0.0138	0.0366	0.0908	0.1093
$Sm_2Zr_2O_7$–(5 vol%, 15 μm)SiC	0.0295	0.0808	0.1489	0.2224
$Sm_2Zr_2O_7$–(10 vol%, 2 μm)SiC	0.1381	0.2341	0.2963	0.3258
$Sm_2Zr_2O_7$–(10 vol%, 10 μm)SiC	0.0387	0.106	0.1523	0.2572
$Sm_2Zr_2O_7$–(10 vol%, 15 μm)SiC	0.1097	0.1778	0.2473	0.2866

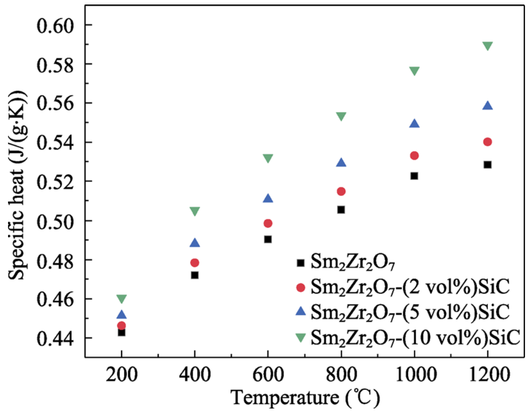

Fig. 5 Specific heat of $Sm_2Zr_2O_7$–SiC composites varying with temperature.

conductivity of $Sm_2Zr_2O_7$–SiC composites with SiC particle size at 2 vol%, 5 vol%, and 10 vol% SiC, respectively. As can be seen from Fig. 6, the photon thermal conductivities of composites decrease first and then increase with the increase of SiC particle size at different temperatures. The composite with SiC particle size of 2 μm has the highest photon thermal conductivity while the composite with SiC particle size of 10 μm has the lowest photon thermal conductivity at different temperatures.

Scattering theory shows that when the particle size is equal to the radiation wavelength, the maximum scattering effect occurs in the ceramic material. The photon wavelengths of gas at high temperatures are mainly concentrated at 1–7 μm. When the particle size of SiC is 2 μm, the influence of SiC on photon scattering is limited, and it has little effect on the photon thermal conductivity of the composites. With the increase of SiC particle size, the photon scattering effect is enhanced. SiC particles with a particle size of

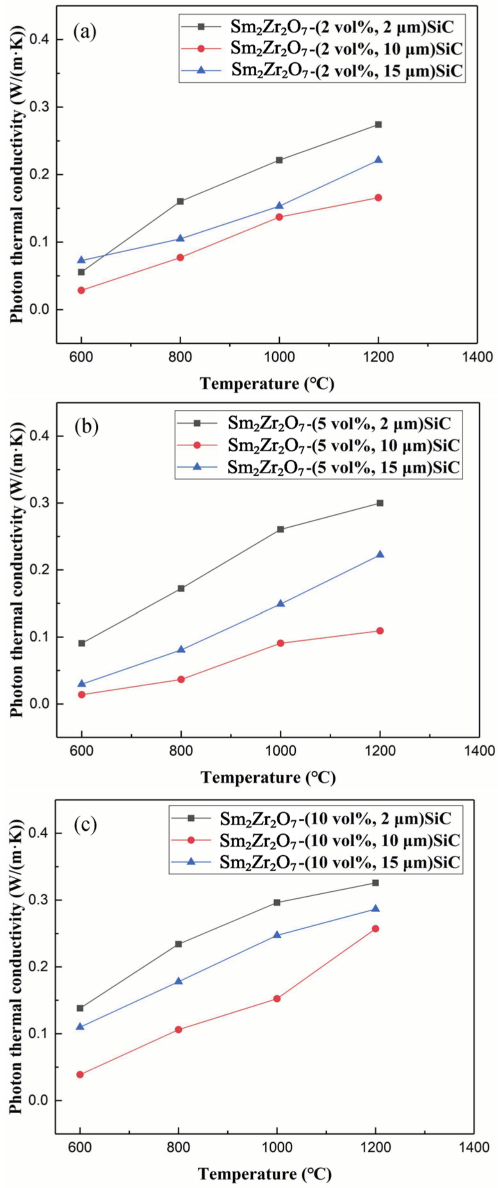

Fig. 6 Photon thermal conductivity of $Sm_2Zr_2O_7$–SiC composites varying with temperature with (a) 2 vol%, (b) 5 vol%, and (c) 10 vol% SiC content.

10 μm are closest to the photon wavelength, which causes the most obvious photon scattering, and the phenomenon of reducing the photon thermal conductivity of the composites is most effective. However, when the size of SiC particles increases to 15 μm, the phenomenon of photon scattering is weakened, which results in that the photon thermal conductivity of the composite material is larger than the photon thermal conductivity of the composites with SiC particle size of 10 μm. Therefore, with the increase of SiC particle size, the photon thermal conductivity of the composite first decreases and then increases, and the composites

with the SiC particle size of 10 μm have the lowest photon thermal conductivity.

Figure 7 shows the photon thermal conductivity of $Sm_2Zr_2O_7$–SiC composites with the SiC content with the SiC particle size 2, 10, and 15 μm, respectively. The photon thermal conductivity of $Sm_2Zr_2O_7$–SiC composites increases with the increase of SiC content when the SiC particle size is 2 μm at different temperatures. When SiC particle size is 10 and 15 μm, respectively, the photon thermal conductivity of $Sm_2Zr_2O_7$–SiC composites decreases first and then increases with the increase of SiC content at different temperatures. The composite of 5 vol% SiC content has the lowest photon thermal conductivity.

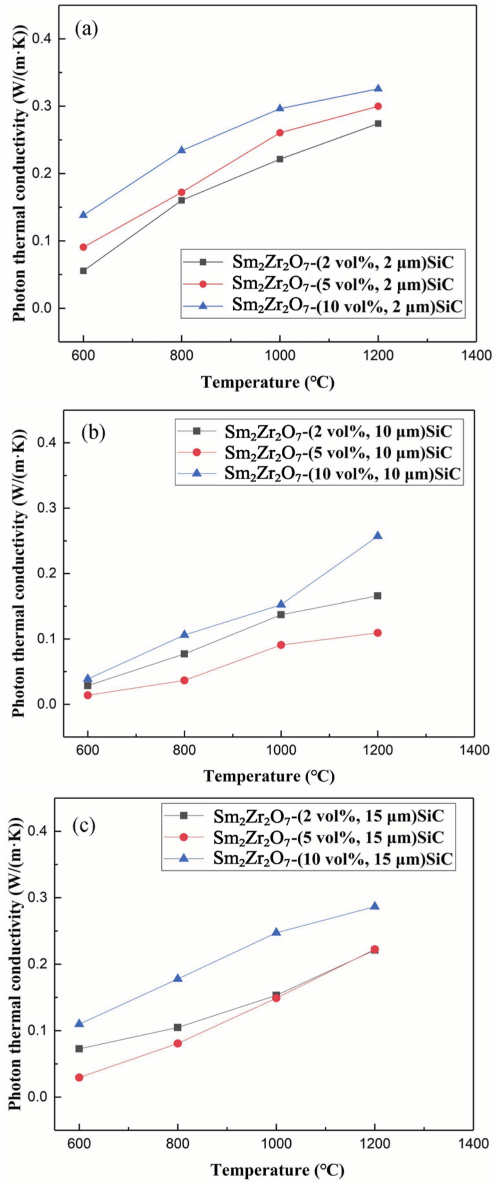

Fig. 7 Photon thermal conductivity of $Sm_2Zr_2O_7$–SiC composites varying with temperature and SiC particle size of (a) 2 μm, (b) 10 μm, and (c) 15 μm.

The thermal conductivity of the composites with the second phase introduced can be approximated as Eq. (4):

$$k = k_1 v_1 + k_2 v_2 \tag{4}$$

where k_1 and k_2 denote the intrinsic thermal conductivities of the matrix and the second phase material, respectively, and v_1 and v_2 denote the volume fraction of the matrix and the second phase material in the composites, respectively. The intrinsic thermal conductivity of SiC is 225 W/(m·K) [14], which is much higher than that of the $Sm_2Zr_2O_7$ matrix. The added SiC will result in higher photon thermal conductivity of the composites than that of $Sm_2Zr_2O_7$. Figure 8 shows the radiation transfer process in different samples. When the size of SiC particle is 2 μm, the effect of SiC on photon scattering is limited. Due to the higher thermal conductivity of SiC, the photon thermal conductivity of the composites increases significantly. The photon thermal conductivity of the composites increases with the increase of SiC content. When the SiC particle size is 10 and 15 μm, the particle size is larger than the photon wavelength of gas at high temperatures, which can cause the photon scattering. The photon scattering caused by SiC increases when the

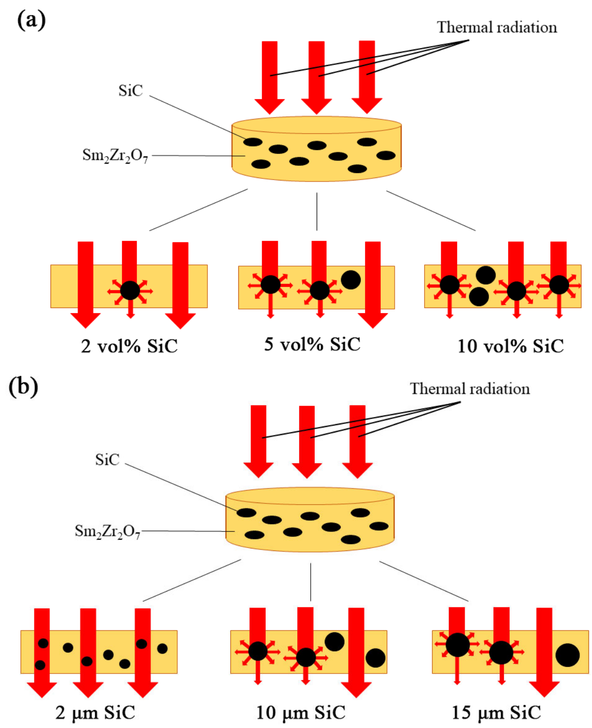

Fig. 8 Schematic diagram of radiation transfer with (a) different SiC content and (b) different SiC size.

SiC content increases from 2 vol% to 5 vol%, and the photon thermal conductivity of the composites decreases. When SiC content is 10 vol%, the photon thermal conductivity of composites increases significantly due to the higher photon thermal conductivity of SiC. Therefore, the composite with SiC content of 5 vol% has the lowest photon thermal conductivity.

The photon thermal conductivity of the composite resulted from the combined effect of the scattering of photons caused by the second phase and the intrinsic photon thermal conductivity of the second phase. When the SiC content is lower, the thermal conductivity of the composites gradually decreases with the increase of the heterogeneous interface. Due to the higher thermal conductivity of SiC, the photon thermal conductivity of the composites increases significantly with the SiC content increases to a certain value. The number of heterogeneous interfaces per unit volume decreases with the SiC particle size in the composite increasing when the SiC content is the same, and thus the carrier scattering ability caused by the second phase decreases. The thermal conductivity of the composite material increases. When the second phase of the proper content and particle size exists in the matrix, the heterogeneous interface introduced by the second phase will enhance the scattering of carriers and effectively block the heat transfer in the material. The $Sm_2Zr_2O_7$–(5 vol%, 10 μm)SiC composite has the lowest photon thermal conductivity. Therefore it is feasible to reduce the photon thermal conductivity by using the heterogeneous interface.

4 Conclusions

In this study, a series of $Sm_2Zr_2O_7$ matrix composites with different volume fraction and particle size of SiC were prepared by hot pressing at 1300 ℃. No other phase exists except for $Sm_2Zr_2O_7$ and SiC in the composites. The photon thermal conductivity of $Sm_2Zr_2O_7$–SiC composites decreases first and then increases with the increase of SiC particle size. For the composites with larger SiC particle size, the photon thermal conductivity decreases first and then increases with the increase of SiC content. $Sm_2Zr_2O_7$–(5 vol%, 10 μm)SiC composite has the lowest photon thermal conductivity comparing with the single-phase $Sm_2Zr_2O_7$, resulting the combined photon scattering caused by SiC and the higher photon thermal conductivity of SiC. The experimental results prove that when the second phase of the proper content and particle size exists in the matrix, it is feasible to reduce the thermal conductivity by using the heterogeneous interface.

Acknowledgements

This study was supported by the National Natural Science Foundation of China (No. 51772027).

References

[1] Vaßen R, Jarligo MO, Steinke T, *et al*. Overview on advanced thermal barrier coatings. *Surf Coat Technol* 2010, **205**: 938–942.

[2] Li F, Zhou L, Liu JX, *et al*. High-entropy pyrochlores with low thermal conductivity for thermal barrier coating materials. *J Adv Ceram* 2019, **8**: 576–582.

[3] Yang G, Zhao CY. Infrared radiative properties of EB-PVD thermal barrier coatings. *Int J Heat Mass Tran* 2016, **94**:199–210.

[4] Wang L, Eldridge JI, Guo SM. Thermal radiation properties of plasma-sprayed $Gd_2Zr_2O_7$ thermal barrier coatings. *Scr Mater* 2013, **69**: 674–677.

[5] Liu ZG, Ouyang JH, Zhou Y, *et al*. Influence of ytterbium- and samarium-oxides codoping on structure and thermal conductivity of zirconate ceramics. *J Eur Ceram Soc* 2009, **29**: 647–652.

[6] Lim G, Kar A. Modeling of thermal barrier coating temperature due to transmissive radiative heating. *J Mater Sci* 2009, **44**: 3589–3599.

[7] Klemens PG, Gell M. Thermal conductivity of thermal barrier coatings. *Mater Sci Eng: A* 1998, **245**: 143–149.

[8] Liu L, Wang FC, Ma Z, *et al*. Thermophysical properties of $(Mg_xLa_{0.5-x}Sm_{0.5})_2(Zr_{0.7}Ce_{0.3})_2O_{7-x}$ (x=0, 0.1, 0.2, 0.3) ceramic for thermal barrier coatings. *J Am Ceram Soc* 2011, **94**: 675–678.

[9] Leitner J, Chuchvalec P, Sedmidubský D, *et al*. Estimation of heat capacities of solid mixed oxides. *Thermochimica Acta* 2002, **395**: 27–46.

[10] Spencer PJ. Estimation of thermodynamic data for metallurgical applications. *Thermochimica Acta* 1998, **314**: 1–21.

[11] Sato Y, Taira T. The studies of thermal conductivity in $GdVO_4$, YVO_4, and $Y_3Al_5O_{12}$ measured by quasi-one-dimensional flash method. *Opt Express* 2006, **14**: 10528–10536.

[12] Ye DL. *Practical Data Manual on Thermodynamics of Inorganic Matter*. Metallurgy Industry Press, 1981. (in Chinese)

[13] Mehling H, Hautzinger G, Nilsson O, *et al*. Thermal diffusivity of semitransparent materials determined by the laser-flash method applying a new analytical model. *Int J*

Thermophys 1998, **19**: 941–949.

[14] Cho TY, Kim YW. Effect of grain growth on the thermal conductivity of liquid-phase sintered silicon carbide ceramics. *J Eur Ceram Soc* 2017, **37**: 3475–3481.